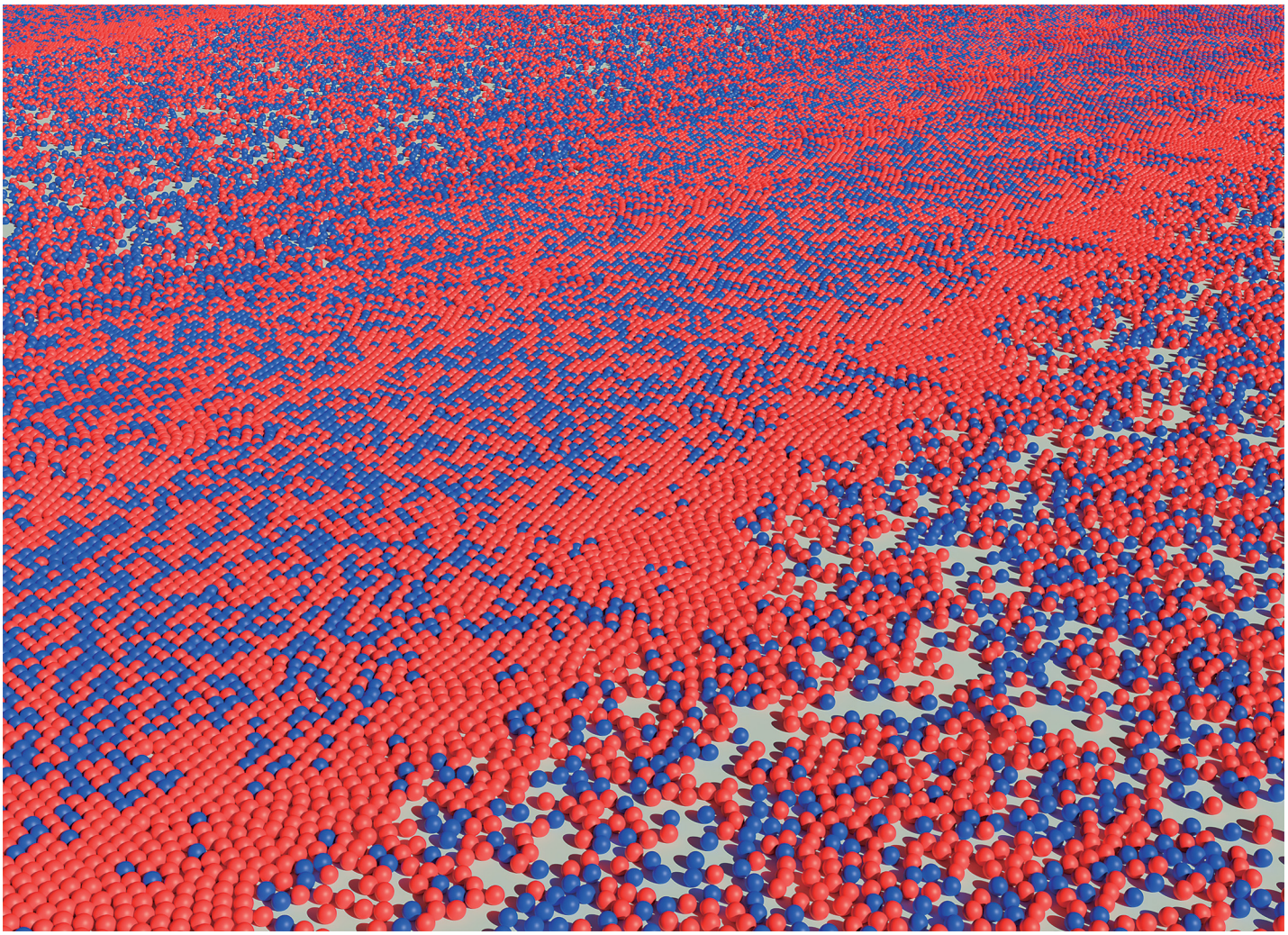

Showcasing research from Professor Valeriani's laboratory, Physics faculty, Universidad Complutense de Madrid, Madrid, Spain.

Dynamics and rupture of doped motility induced phase separation

The image is an artistic representation of a Motility-Induced Phase Separation (MIPS) slab in a binary mixture of active (red) and passive (blue) particles under periodic boundary conditions. Unlike purely active systems, the introduction of a small number of passive particles breaks the symmetry of the MIPS band, producing a well-defined interface propagation, which is not merely a rigid shift or a source–sink effect, but rather a self-sustained combination of both.

Image reproduced by permission of Chantal Valeriani from *Soft Matter*, 2025, **21**, 5413.

As featured in:

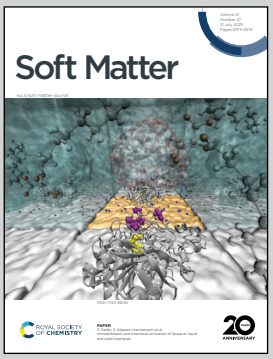

See Rodrigo Fernández-Quevedo García, Chantal Valeriani *et al.*, *Soft Matter*, 2025, **21**, 5413.

ROYAL SOCIETY OF CHEMISTRY

rsc.li/soft-matter-journal

Registered charity number: 207890

Soft Matter

PAPER

View Article Online
View Journal | View Issue

Cite this: *Soft Matter*, 2025, **21**, 5413

Dynamics and rupture of doped motility induced phase separation†

Rodrigo Fernández-Quevedo García,*[ab] Enrique Chacón,[c] Pedro Tarazona[d] and Chantal Valeriani *[ab]

Adding a small amount of passive (Brownian) particles to a two-dimensional dense suspension of repulsive active Brownian particles does not affect the appearance of a motility-induced phase separation into a dense and a dilute phase, caused by the persistence of the active particles' direction of motion. Unlike a purely active suspension, the dense slab formed in an elongated system of a passive–active mixture may show, over long periods of time, a stable and well-defined propagation of the interfaces, because of the symmetry breaking caused by the depletion of passive particles on one side of the slab. We investigate these dynamical structures *via* average density profile calculations, revealing an asymmetry between the two interfaces, and enabling a kinetic analysis of the slab movement. The apparent movement of the dense slab is not a pure source/sink effect, nor a rigid displacement of all the particles, but a self-sustained combination of both effects. Furthermore, we analyse the specific fluctuations that produce, cancel and abruptly reverse the slab motion.

Received 6th February 2025,
Accepted 13th May 2025

DOI: 10.1039/d5sm00134j

rsc.li/soft-matter-journal

1 Introduction

One of the simplest theoretical models proposed to unravel the features of the collective behaviour of active particles is the so-called active Brownian particle (ABP) model, consisting of self-propelling Brownian particles which gradually change their direction of motion.[1–4] Numerical simulations of suspensions of repulsive ABPs have demonstrated that ABPs spontaneously aggregate due to the persistence of particles' direction of motion, undergoing a motility induced phase separation (MIPS)[5–9] into a dense and a dilute phase.[3,5,9–17] These numerical results have been supported by phase-field calculations[18–21] and experimental results on two-dimensional suspensions of active colloids.[22–25]

When MIPS takes place in numerical simulations, dealing with an elongated cylindrical box allows for characterizing its structural features, such as its interfacial properties. As suggested by the authors of ref. 26, considering the swim pressure as a contribution to the total pressure results in a negative interfacial tension. However, different from equilibrium, this leads to a long-time stable MIPS. Patch and coworkers[27] have addressed the controversy of a negative surface tension coexisting with a stable interface by discovering a Marangoni-like effect arising from the presence of sustained tangential currents at the interfaces (on both dilute and dense phases). By means of a continuum description, the authors of ref. 28 demonstrated that modelling activity as a spatially varying force allows one to predict consistent pressures and nearly zero surface tension.

Hermann and coworkers[29] implemented non-equilibrium generalization of the microscopic treatment of the interface, leading to a positive interfacial tension that directly explained the stability of the interface. The approach in ref. 29 produces the "intrinsic density profile".[30] Thus, one could study capillary wave fluctuations and the wave vector dependence of the interfacial tension. Some of us have recently analysed the features of the dense/dilute interfaces in terms of intrinsic density and force profiles, calculated by means of Capillary Wave Theory.[31] In our work, we attributed the MIPS stability to the local rectification of the random active force acting on particles at the dense (inner) side of the MIPS interface. This caused an external potential producing a pressure gradient across the interface and led us to conclude that the MIPS mechanical surface tension could not be described as the surface tension of equilibrium coexisting phases.

The stability of MIPS has been tested against several features. On the one side, hydrodynamics, together with the particles' shape, has been shown to affect the existence of MIPS. MIPS is suppressed when particles are spherical,[32] while

[a] *Departamento de Estructura de la Materia, Física Térmica y Electrónica, Universidad Complutense de Madrid, 28040 Madrid, Spain. E-mail: rodfer05@ucm.es, cvaleriani@ucm.es*
[b] *GISC – Grupo Interdisciplinar de Sistemas Complejos, 28040 Madrid, Spain*
[c] *Instituto de Ciencia de Materiales de Madrid (ICMM), Consejo Superior de Investigaciones Científicas (CSIC), Campus de Cantoblanco, 28049 Madrid, Spain*
[d] *Departamento de Física Teórica de la Materia Condensada, Condensed Matter Physics Center (IFIMAC), Universidad Autónoma de Madrid, 28049 Madrid, Spain*

† Electronic supplementary information (ESI) available. See DOI: https://doi.org/10.1039/d5sm00134j

it is enhanced when particles are elongated.[33] MIPS is also hindered in the case of a suspension of chemotactic active Brownian particles.[34] In contrast, MIPS is neither hindered when particles' equations of motion are characterised by inertia[35,36] nor when particles' motion is on-lattice[37,38] rather than off-lattice.

Adding passive particles to an ABP suspension, one could study the physics of a binary mixture. By means of experiments or numerical simulations, mixtures of active and passive particles have been studied by several authors.[39–46] When focusing on the behaviour of passive particles, active particles (whether ABP or bacteria) influence not only the structural arrangement of passive particles, but also their dynamic properties, as demonstrated in ref. 41–46. On the other side, adding a small amount of passive particles to a suspension of active particles[18,47,48] is not enough to impede MIPS from taking place but can alter its morphology. When MIPS appears, the dense phase is not homogeneous anymore, since active particles are more concentrated at the boundaries and passive ones are mostly concentrated at its inner part. Interestingly, the fluctuations of the MIPS interface are much more pronounced in the binary mixture than in the purely active system.[47] In this respect, Wysocki and coworkers[18] studied an active/passive binary mixture in a two-dimensional elongated simulation box and identified a collective motion of the dense MIPS phase. This collective motion, completely absent in the purely active ABP suspension,[48] consisted of well-defined propagating interfaces caused by a flux imbalance of the active and passive particles in the dilute phase.

In the present work, we investigate the behaviour of a two-dimensional binary mixture of repulsive (WCA) active (A)/passive (P) Brownian particles *via* simulations by means of the LAMMPS Molecular Dynamics package.[49] The active Brownian particles, at temperature T, with Boltzmann constant k_B, translational diffusion coefficient D_t, and the stochastic uncorrelated white noise $\vec{\xi}_i$, have velocities given by

$$\dot{\vec{r}}_i = \frac{D_t}{k_B T}\left(-\sum_{j\neq i}\vec{\nabla}U(r_{ij}) + |F_a|\vec{n}_i\right) + \sqrt{2D_t}\vec{\xi}_i, \qquad (1)$$

where on top of the interaction with all other particles, through the pair potential $U(r)$, one should consider a constant self-propelling force, F_a, whose direction is given by the unitary vector $\vec{n}_i = (\cos\theta_i, \sin\theta_i)$, with angle θ_i changing independently for each particle,

$$\dot{\theta}_i = \sqrt{2D_r}\eta_i, \qquad (2)$$

with the rotational diffusion coefficient, D_r, and the stochastic uncorrelated white noise η_i.

Using the same equation (eqn (1)), the passive particles are simulated by setting $F_a = 0$. The interaction potential in the first term of eqn (1), without a distinction between the active or passive character of particles, is chosen as the repulsive WCA potential,[50]

$$U(r) = \begin{cases} 4\varepsilon\left(\left(\frac{\sigma}{r}\right)^{12} - \left(\frac{\sigma}{r}\right)^{6}\right) + \varepsilon & r < 2^{1/6}\sigma \\ 0 & r > 2^{1/6}\sigma \end{cases} \qquad (3)$$

where r is the distance between the centre of two particles and ε is the minimum value of the well of a Lennard-Jones potential. All quantities presented in this paper are expressed in reduced units, in terms of σ and ε. The time step for Brownian dynamics simulations is fixed at $\delta t = 5 \times 10^{-5}$, and simulations typically run for up to 5×10^3 time units, with longer runs (10^4) performed when higher statistical accuracy is required.

In our simulations, we keep the area A applying periodic boundary conditions in a box with lengths $L_x > L_y$ (as in ref. 47). The periodicity along the short edge (L_y) plays the usual role of avoiding finite size effects; however, on the long edge (L_x) its role should be regarded as a system with a real cylindrical geometry. We set the number of active (N_A) and passive (N_P) particles constant so that the total number of particles is $N_T = N_A + N_P$. Unless explicitly stated otherwise, we set $N_T = 8055$ with a box size of $L_x = 200\sigma$ and $L_y = 50\sigma$, where σ denotes the particle diameter. The passive particle concentrations vary from $\eta_P = N_P/N_T = 0.4$ down to the purely active system ($\eta_P = 0$). Throughout the study, the number density is fixed at $\rho = N_T/(L_xL_y) = 0.8055$. Almost most of the results correspond to the standard system size ($L_x = 200\sigma$, $L_y = 50\sigma$, and $N_T = 8055$). However, when explicitly indicated, we will also present results for other system sizes.

The activity is controlled *via* the Peclet number, defined as $P_e = 3\nu\tau_r/\sigma$, where $\nu = F_aD_t/k_BT$ is the self-propulsion velocity and $\tau_r = 1/D_r$ is the reorientation time. We set $D_t = 1.5$, $D_r = 0.6$, $k_BT = 1.5$, and $F_a = 24$, resulting in $P_e = 120$. This choice of density and Peclet number guarantees phase separation (MIPS) for both the pure system ($\eta_P = 0$) and the mixtures studied here, up to $\eta_P = 0.4$.[47,48]

2 Characterization of the dense slab motion

Typical MIPS snapshots, separated by $\Delta t = 100$ time intervals (from top to bottom) are reported in Fig. 1 for the pure $\eta_P = 0$ system (left) and the $\eta_P = 0.4$ mixture (right), (see also Videos Vid_SP_mov_MIX_00.mp4 and Vid_SP_mov_MIX_04.mp4, ESI†).

The MIPS in the pure system of ABP (left panels) forms a dense slab (or band) closing itself over the L_y (shorter) period, and filling a fraction L_s/L_x of the (horizontal, in the Figure) X axis. The less dense phase fills the rest ($(L_x - L_s) \times L_y$) of the simulation box. The periodic boundary along X implies that the dense band may appear at any position, even apparently split into two pieces, at the opposite ends of the $0 \leq x \leq L_x$ box. As usual in phase separations, the thickness of each region would readjust to the values of N_T and the area $A = L_x \times L_y$, without a change in the coexisting densities.

For the $\eta_P = 0.4$ mixture (right column in Fig. 1) the snapshots show also the formation of a dense slab, although thinner than at the left column because in the mixture there is less density difference between the two phases. That could be expected since the active particles are diluted (keeping the same total density) in the mixture with passive particles. The fluctuations at the interfaces are larger in the mixture than in

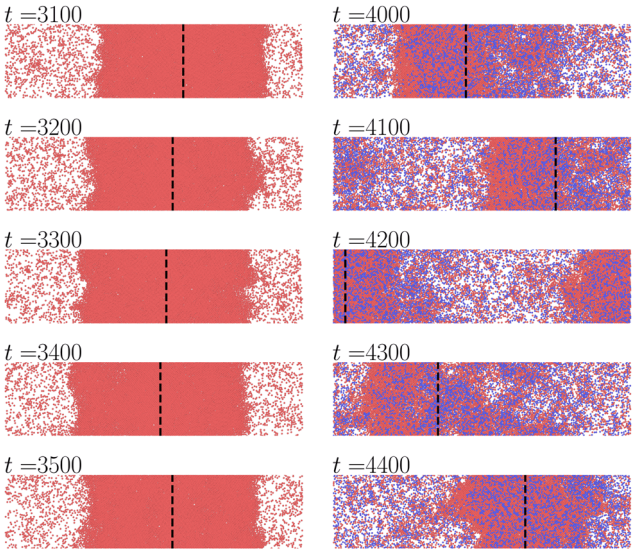

Fig. 1 Top: MIPS snapshots for η_P = 0 (left-hand side) and η_P = 0.4 (right-hand side) (active particles in red and passive ones in blue). The time difference between the top and bottom snapshots is Δt = 100 (time indicated in each frame). The black dashed lines mark the position of the slab's center of mass.

the pure ABP system, but the most important difference comes in the series of snapshots along each column (see also the Videos, ESI†).

In the pure active system, the dense MIPS band has a slow random wandering along the X direction, while in the mixture there is fast translation of the band along the X direction, either to the right (as shown in these snapshots) or to the left (at other times along the simulation). The same sense of motion is kept over long time periods and the band often goes across the periodic boundary x = 0, L_x.

As shown below, this self-sustained movement relies on the inhomogeneity of the whole system along the X direction, including a clear asymmetry between the interfacial structures

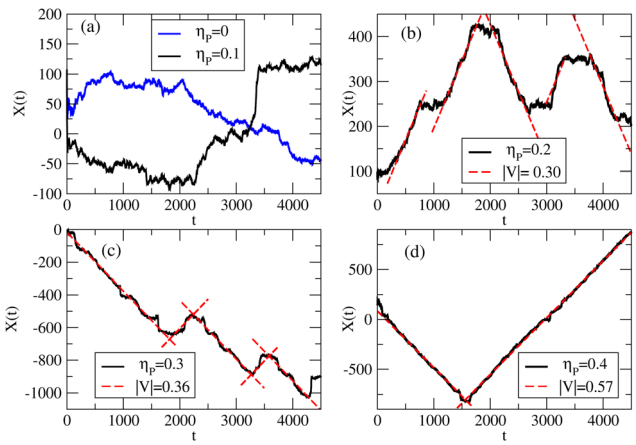

Fig. 2 Slab position over time, $X(t)$, for various η_P values (Panel (a) shows η_P = 0 and 0.1, while panels (b), (c), and (d) correspond to η_P = 0.2, 0.3, and 0.4, respectively.). Red dashed lines indicate periods of linear displacement, with slopes (velocities $|V|$) also shown in the legend.

at the two edges of the moving slab. That contrasts with the homogeneous phases in the MIPS of pure ABP systems, in which the inhomogeneity is restricted to the two symmetric interfacial regions.

The formation of inhomogeneous structures with steady movement is known for systems of Brownian interacting particles kept (by an external force) in steady motion with respect to the bath, so that the balance between the friction, the external force and the interactions creates inhomogeneous "front" and "wake" structures along the direction of motion.[51]

The use of periodic boundary conditions along the X axis (perpendicular to the interfaces) becomes then a physical choice (like in a real cylindrical or toroidal geometry), rather than a computational trick, since the values of L_x and L_s (that is controlled by $N_{T)}$ affect the whole inhomogeneous structure. Taking L_x as a physical period allows us to explore steady states in which the inhomogeneous density distributions move (over long time periods) without changing their mesoscopic structure.

Our analysis, under these simplified conditions, aims to quantify the (visually observed) difference between pure and mixed systems. The relevance of more complex mesoscopic MIPS structures in mixtures under other geometrical constraints will be discussed later.

First, we need a quantitative mesoscopic description for the motion of these structures, averaging over the rapid changes of the particle positions x_i (for i = 1, N_T). To that effect, we define (see the ESI† for discussion on alternative definitions) the instantaneous position of the dense band $X(t)$ as‡

$$X(t) = \frac{L_x}{2\pi}\arctan\left(\frac{\sum_{i=1}^{N}\sin\left(\frac{2\pi}{L_x}x_i(t)\right)}{\sum_{i=1}^{N}\cos\left(\frac{2\pi}{L_x}x_i(t)\right)}\right), \quad (4)$$

that corresponds to getting real positive values for the lowest ($q = 2\pi/L_x$) Fourier component of the particle position $\sum_{i=1}^{N_T} e^{iq(x_i(t)-X(t))}$; so that $X(t)$ is located at the center of the dense slab, independent of the position of the slab in the $0 \le x \le L_x$ interval.

The results for $X(t)$, reported in Fig. 2, are then used to calculate the velocity of the slab as a mesoscopic structure.

$$V(t) = \frac{dX(t)}{dt} \approx \frac{X(t+\Delta t) - X(t)}{\Delta t}, \quad (5)$$

with time step $\Delta t = 0.05 = 10^3\delta t$.

Then $V(t)$ is averaged as $\langle V\rangle$, over $250\Delta t = 12.5$ time intervals, and used to get its autocorrelation (ESI†), $\langle (V(t_o) - \langle V\rangle)(V(t_o + t) - \langle V\rangle)\rangle \approx \Delta V^2 \exp(-t/\tau_p)$, to characterize rapid fluctuations with persistence time $\tau_p \approx 1.8 \pm 0.2$, that we find to be similar in pure and mixed systems.

For the unbiased random walk (η_P = 0) there is no longer time scale than τ_p, so that the mean square amplitude of the

‡ Along the simulation we chose the branch of the arc-tangent in which $X(t)$ is the closest to its previous position $X(t - \delta t)$, in order to keep the number full L_x rounds.

$V(t)$ fluctuations $\Delta V^2 \equiv \langle (V(t) - \langle V \rangle)^2 \rangle$ should produce a random walk of $X(t)$ with diffusion constant $D = \Delta V^2 \tau_p \approx 0.3 \pm 0.05$; consistent with the observed changes $\Delta X(t) \sim \pm 50$ over the full simulation run $t_{max} = 4400$. Such a slow drift (that should be size dependent) is typical in any phase separation and it is usually dealt with (small) rigid shifts of all particle positions to keep the dense slab at an approximately fixed position in the periodic cell.

In contrast, mixtures with $\eta_p \geq 0.2$ (Fig. 2, panels b–d) show long steady motion periods (SMPs), marked as red dashed lines, with a nearly constant (either positive or negative) slope $X(t) - X(t_o) \approx \pm V_{SMP}(\eta_P)(t - t_o)$, with (absolute) values of the slope that increase from $V_{SMP}(0.2) \approx 0.30$ to $V_{SMP}(0.4) \approx 0.57$. The mean square fluctuations $\Delta V^2 = \langle (V(t) - \langle V(t) \rangle)^2 \rangle \approx 0.3$ (over the same 12.5 time intervals) are just slightly larger than for $\eta_P = 0$.

The amplitude $\sqrt{\Delta V^2} \approx 0.5$ of these fast $\tau_p \approx 1.8$ fluctuations are of the same order of magnitude as the mean value V_{SMP}; however, the SMP are clearly identified in $X(t)$ (see Fig. 2) and also in the histograms for $V(t)$, (ESI†) because a much longer time scale emerges, with a typical SMP persistent time τ_{SMP} that we can only estimate to be $\tau_{SMP} \sim 500$ for $\eta_P = 0.2$, $\tau_{SMP} \sim 1000$ for $\eta_P = 0.3$ and larger for $\eta_P = 0.4$.

The SMPs are interrupted by large fluctuations in the structure of the MIPS slab, reflected in sharp changes of the nominal position $X(t)$ defined in eqn (4). Then, there may be a rest period, in which $X(t)$ fluctuates without forth-back bias before a new sudden change in $X(t)$ leads to start a new SMP, that may be in the opposite direction (with a U-turn of the slab) or in the same direction as the previous SMP. We may estimate that for $\eta_P = 0.4$ there is a typical time $\tau_o \sim 100$ (just an order of magnitude) for the rest period between two SMPs. U-turns occur at each η_p during periods of steady motion. As η_p increases, the time required for a U-turn to develop becomes shorter. Thus, at $\eta_p = 0.4$, the U-turn is very abrupt. In this respect, given sufficient simulation time, a U-turn d also occurs at $\eta_p = 0.3$, although less sharply than at $\eta_p = 0.4$, but still more sharply than at $\eta_p = 0.2$.

Therefore, for that high concentration of passive particles $\tau_p \ll \tau_o \ll \tau_{SMP}$ gives a good separation of time scales for our analysis of the SMPs. For lower η_P values, τ_o increases while τ_{SMP} decreases, so that for $\eta_P = 0.2$ we may estimate $\tau_o \sim \tau_{SMP} \sim 500$.

Notice that we have only very crude estimations for $\tau_{SMP}(\eta_P)$ and $\tau_o(\eta_P)$ since good statistics would require extremely long simulation runs. As in any mesoscopic characterization there are uncertainties; a red line in Fig. 1 may go through a large fluctuation, and we could take it as a single SMP or as two successive SMPs that keep the same direction of motion, after a very short rest time.

Nevertheless, we find robust indications for the emergence of the time scales $\tau_{SMP} > \tau_o \gg \tau_p$, leading to superdiffusive behaviour of the dense MIPS clusters, as a peculiarity of active–passive mixtures and the subject of our study. In the remaining of our work, we will focus on the $\eta_P = 0.4$ case for a detailed analysis, because it provides the best statistics to characterize the structures that produce the SMP.

However, similar behaviour is clearly observed for $\eta_p = 0.3$ and 0.2. For $\eta_P = 0.1$ we observe sudden changes in $X(t)$, that do not appear in the pure ($\eta_P = 0$) MISP slabs, but the time scale separation between SMP and rest periods becomes uncertain.

3 Analysis of the density and current profiles

The instantaneous density profiles $\hat{\rho}_\alpha(x,t) = \sum_{i=1}^{N_\alpha} \delta(x - x_i(t))/L_y$, for α = A, P particles, should be averaged over a time interval $t \in [t_o, t_o + \Delta t]$ to get smooth mean density profiles $\rho_\alpha(x) = \langle \hat{\rho}_\alpha(x,t) \rangle_{\Delta t}$. However, the fast movement of the band in active–passive mixtures leads to flat $\rho_\alpha(x)$, unless the time average is chosen to be very narrow, with the consequence of being too noisy $\rho_\alpha(x)$. This problem can be overcome by evaluating the shifted density profiles[5,12]

$$\tilde{\rho}_\alpha(x) = \frac{1}{L_y} \left\langle \sum_{i=1}^{N_\alpha} \delta(x + X(t) - x_i(t)) \right\rangle_{\Delta t}. \quad (6)$$

The emergent time scale separation allows to take $\tau_{SPM} > \Delta t \gg \tau_p$ with a very good average over the rapid fluctuations, but still within a single SMP. Thus, for $\eta_p = 0.4$, over a period with $\langle V(t) \rangle \approx +0.57$ we obtain the strongly asymmetric $\tilde{\rho}_A(x)$ and $\tilde{\rho}_P(x)$ profiles shown in Fig. 3.

At the back of the moving band, $\tilde{\rho}_A(x)$ (dashed red) presents a peak and $\tilde{\rho}_P(x)$ (dashed orange) drops to a narrow minimum. In contrast, at the front, $\tilde{\rho}_A(x)$ and $\tilde{\rho}_P(x)$ have similar smoother decays. For comparison, the pure ABP system (black line) presents a fairly symmetric profile and a larger MIPS density difference.

The same qualitative features are found at lower concentrations of passive particles, as shown in Fig. 4, for $\eta_P = 0.2$.

In panels (b) and (c) eqn (6) is averaged over the SMP with $\langle V(t) \rangle \approx \pm 0.30$, respectively (along the periods marked as red-dashed lines in Fig. 2(b)). The asymmetry is $(\tilde{\rho}_\alpha(x) \to \tilde{\rho}_\alpha(-x))$ in SMP with the opposite velocity. The rest periods ($\langle V(t) \rangle \approx 0$) are now long enough to take good averages, that give the symmetric density profiles in Fig. 4(a). Notice that the steady motion of the

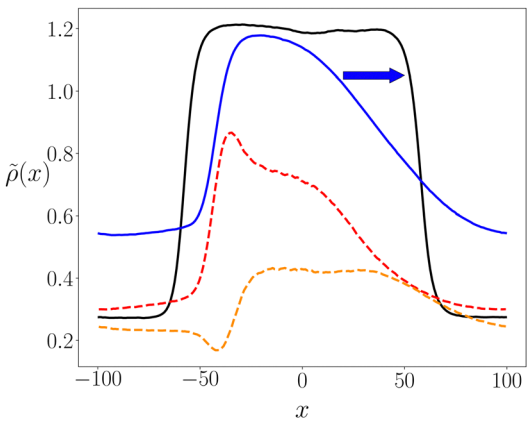

Fig. 3 Full lines: mean total density profile $\tilde{\rho}(x)$: for $\eta_P = 0$ (black) and 0.4 (blue). For the latter, dashed lines: $\tilde{\rho}_A(x)$ (red) and $\tilde{\rho}_P(x)$ (orange); blue arrow: the direction of motion in the SMP used for the time average.

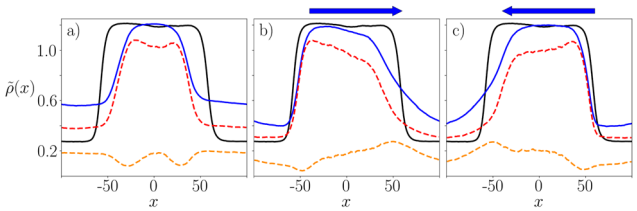

Fig. 4 Full lines: mean total density profiles (eqn (6)) for $\eta_P = 0.2$; blue line: total density, red-dashed line: $\tilde{\rho}_A(x)$ and orange-dashed line: $\tilde{\rho}_P(x)$. For comparison, the black liners give the density profile in a pure ($\eta_P = 0$) ABP system with the same ρ_T. In panel (a) the average is taken over the rest periods ($\langle V(t)\rangle \approx 0$ in panel (b) of Fig. 2); in panels (b) and (c) the profiles are averaged over the SMP (red-dashed lines in Fig. 2) when the slab moves in the direction of the top blue arrow.

band across the system seems to reinforce (rather than to weaken) the MIPS in the mixture, since the density contrast between the maximum density (at $x \approx 0$) and the minimum density (at $x \approx \pm L_x/2$) is higher in the SMP asymmetric profiles, than in the symmetric profiles during the rest periods.

Wysocki *et al.*[18] proposed a source-sink mechanism to explain the band displacement, where the receding interface acts as a source, evaporating particles into the dilute phase, while the advancing front, acting as a sink, captures particles into the dense phase. A representation of this source/sink effect is reported in Fig. 5 for $\eta_P = 0.4$, with four snapshots, each with $X(t)$ as a vertical dashed line and the MIPS boundaries as wavy black lines.

In the top snapshot, particles are coloured in red if close to the source (back) side and in purple if close to the sink (front). From top to bottom, the red particles rapidly escape from the back interface and are added at the front interface. The purple particles remain mostly stationary as the slab moves through them, diffusing slowly within the dense region.

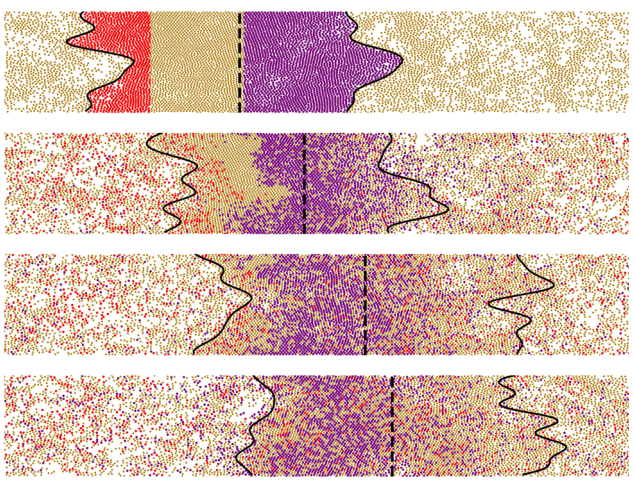

Fig. 5 Snapshots showing the slab's movement as a function of time (from top to bottom). Slab boundaries[31] underlined by a black line as well as the mass centre position, $X(t)$ (vertical dashed line). Top snapshot: Slab particles on each side are coloured red (source interface) and purple (sink interface). Their colour is maintained in the all snapshots, showing how particles change position with time.

For quantitative analysis, we use Smoluchowski's equation for the instantaneous distributions of density $\rho(\vec{r},t) = \langle\delta(\vec{r} - \vec{r}_i(t))\rangle_n$ and current $\vec{j}(\vec{r},t) = \langle\delta(\vec{r} - \vec{r}_i(t)\vec{v}_i(t))\rangle_n$, smoothed by the average $\langle\ldots\rangle_n$ over many realizations of the Brownian noise acting on the particles. Along a SMP the velocity of the MIPS band has rapid ($\sim\tau_p$) fluctuations around a mean value $\langle V\rangle$. We assume that the self-averaging of $\tilde{\rho}(x)$ gives $\rho(\vec{r},t) = \rho(x,t) \approx \tilde{\rho}(\tilde{x})$, with $\tilde{x} = x - \langle V\rangle t$, and the continuity equation for the steady state movement of the band becomes[51] $\partial_t\rho_\alpha(x,t) = -\partial_x j_\alpha(x,t) = -\langle V\rangle\partial_{\tilde{x}}\tilde{\rho}(\tilde{x})$, that may be integrated to the current densities

$$j_\alpha(\tilde{x}) = \langle V\rangle\tilde{\rho}_\alpha(\tilde{x}) - \Delta_\alpha \qquad (7)$$

where the integration constant, Δ_α, is the counter-current which makes $j_\alpha(\tilde{x})$ to be lower than the apparent current carried by the moving slab.

In our simulations, we get Δ_A and Δ_P from $\langle V\rangle$ and the mean velocity of the particles, for each species,

$$\langle v_\alpha\rangle \equiv \frac{1}{N_\alpha}\left\langle\sum_{j=1}^{N_\alpha} v_i\right\rangle = \frac{\int_0^{L_x}\mathrm{d}x j_\alpha(x,t)}{\int_0^{L_x}\mathrm{d}x\rho_\alpha(x,t)} = \langle V\rangle - \frac{\Delta_\alpha}{\langle\rho_\alpha\rangle} \qquad (8)$$

where $\langle\rho_\alpha\rangle = N_\alpha/(L_xL_y)$ are the fixed mean densities. For $\eta_P = 0.4$ and $\langle V\rangle \approx 0.57$ (as in Fig. 3) we get $\langle v_A\rangle = -0.03$ and $\langle v_P\rangle = 0.05$, which correspond to counter currents, $\Delta_P \approx 0.17$ and $\Delta_A \approx 0.29$.

4 Brownian dynamics analysis for the SMP

In the Smoluchowski equation for Brownian particles (with mobility Γ, temperature T and translational diffusion constant $D_t = kT\Gamma$) the (noise averaged) currents for each species are

$$j_\alpha(x,t) = \Gamma\left(\sum_{\beta=A,P} f_{\alpha\beta}(x,t) - kT\partial_{\partial x}\rho_\alpha(x,t) + \delta_{\alpha A}f^a(x,t)\right) \qquad (9)$$

with the interaction force densities $f_{\alpha\beta}(x,t)$ that particles of species α receive from particles of species β, the thermal diffusion (both for active and passive particles), and the active force density $f^a(x,t)$ (with $\delta_{AA} = 1$ and $\delta_{BA} = 0$), which reflects the local rectification of the (independently random but slowly varying) active force acting on each particle.

All these force densities may be evaluated in our simulations, and averaged along a SMP in terms of the relative position $x = x_i(t) - X(t)$ of each particle from the mesoscopic position of the slab, as done in eqn (6) for the density profile $\tilde{\rho}_\alpha(x)$. The results in Fig. 6 correspond to the same SMP, for $\eta_P = 0.4$, as the density profiles in Fig. 3.

The assumption $\rho(x,t) \approx \tilde{\rho}(\tilde{x})$, with $\tilde{x} = x - \langle V\rangle t$, that leads to eqn (7) may now be used for each component of the force densities $f_\alpha(x,t) \approx \tilde{f}_\alpha(\tilde{x})$, to take the time averages along a SMP with mean slab velocity $\langle V\rangle$ as (self-averaging) representation of

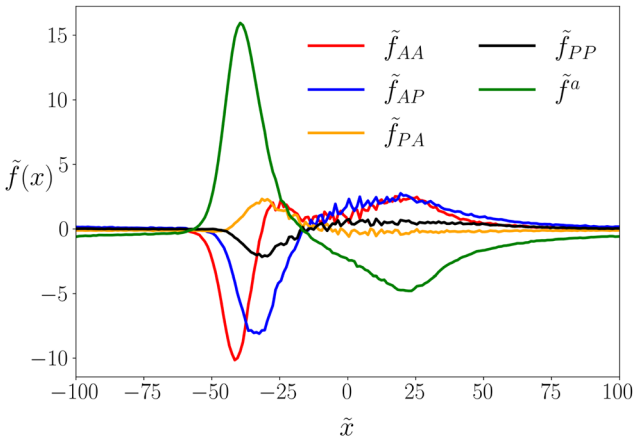

Fig. 6 Mean force profiles for the system with $\eta_P = 0.4$ moving towards the positive X-axis: the interaction between active–active, $\tilde{f}_{AA}$ (red), and passive–passive, $\tilde{f}_{PP}$ (black), active–passive, $\tilde{f}_{AP}$ (blue), and the opposite $\tilde{f}_{PA}$ (orange); and the active force density profile, $\tilde{f}^{a}$ (green).

the Brownian noise average in Smoluchowski eqn (9), to get

$$j_\alpha(\tilde{x}) = \Gamma\left(\sum_{\beta=A,P} f_{\alpha,\beta}(\tilde{x}) - kT\partial_{\tilde{x}}\tilde{\rho}_\alpha(\tilde{x}) + \delta_{\alpha A} f^{a}(\tilde{x})\right). \quad (10)$$

Fig. 7 shows a comparison of (again for the same $\eta_P = 0.4$ SMP analyzed in Fig. 3) the mean velocities, $v_\alpha(\tilde{x}) \equiv j_\alpha(\tilde{x})/\rho_\alpha(\tilde{x})$, obtained *via* eqn (7) (*i.e.* from the density profile, the global mean velocities $\langle v_\alpha\rangle$ and the slab $\langle V\rangle$) and *via* eqn (10) with the force densities in Fig. 6.

The fairly good agreement between the kinetic and the dynamical results (see also in the ESI† the direct comparison for $j_\alpha(\tilde{x})$) gives a strong support to our assumption $j(x,t) \approx \tilde{j}(\tilde{x})$, *i.e.* to the self-averaging of the Brownian thermal noise as time averages over the SMP. Therefore we may proceed with the following dynamical interpretation for the structural origin of the SMP based on (10).

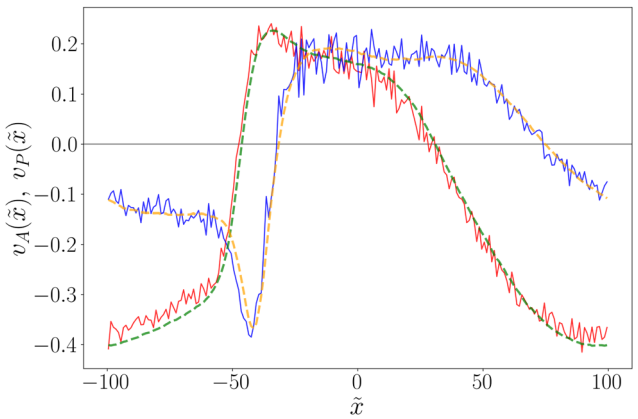

Fig. 7 Particle velocity profiles for $\eta_P = 0.4$ calculated *via* eqn (7). Using the currents from the forces (noisy solid lines) and the density profiles (dashed lines). Both the profiles of active (red and green lines) and passive (blue and orange lines) particles are included. The horizontal line represents $v_A(\tilde{x}) = v_P(\tilde{x}) = 0$.

Eqn (7) and (10) give

$$\Delta_\alpha = \langle V\rangle\rho_\alpha(\tilde{x}) - \Gamma\left(\sum_{\beta=A,P} f_{\alpha,\beta}(\tilde{x}) - kT\partial_x\rho_\alpha(\tilde{x}) + f^{a}(\tilde{x})\right). \quad (11)$$

The constant value of the right-hand side, independent of $\tilde{x}$, is a strong link between the results for the density and force profiles when the system is in an SMP. Moreover, taking the average of (11) over the total length $0 \le \tilde{x} \le L_x$, with periodic boundaries, the contributions from the Brownian diffusion and the active force (both with an independent random direction on each particle) are null.

The same applies to the repulsion between particles of the same species $f_{AA}(\tilde{x})$ and $f_{PP}(\tilde{x})$ that have null integrals. The qualitative difference of a mixture with respect to a pure ABP system is that the integrals of $f_{AP}(\tilde{x})$ and $f_{PA}(\tilde{x})$,

$$\frac{1}{L_x}\int_0^{L_x} \mathrm{d}x f_{PA}(t) = -\frac{1}{L_x}\int_0^{L_x} \mathrm{d}x f_{AP}(t) \equiv \frac{F_{PA}}{A} = -\frac{F_{AP}}{A}, \quad (12)$$

may have non-null (but opposite) values reflecting that, if the density profiles break the left–right symmetry, the active particles may globally push (and be pushed back by) the passive ones. The static (on average) centre of mass for the whole system, which emanates from the Brownian dynamics and the mean average of the active force on each particle, imposes that $N_A\langle v_A\rangle + N_P\langle v_P\rangle = 0$.

As observed in our simulations, the global movement of the two species has to be in opposite directions, and it is fully determined by their mutual global force $F_{PA} = -F_{AP}$. The counter currents in eqn (7) may be obtained in terms of the total forces between active and passive particles,

$$\Delta_\alpha = \langle V(t)\rangle\langle\rho_\alpha\rangle - \Gamma\frac{F_{PA}}{A}, \quad (13)$$

which amounts to the dynamical balance for the global mean velocity of each species

$$\langle v_P\rangle = \Gamma\frac{F_{PA}}{N_P} \quad \text{and} \quad \langle v_A\rangle = -\Gamma\frac{F_{PA}}{N_A} \quad (14)$$

and the static (on average) centre of mass for the whole system, $N_A\langle v_A\rangle + N_P\langle v_P\rangle = 0$. The global movement of the two species has to be in opposite directions, and it is fully determined by their mutual global force $F_{PA} = -F_{AP}$. The counter currents of the two species are linked by the restriction $\Delta_A + \Delta_P = \langle V\rangle\rho_T$, with ρ_T being the total density.

The velocity profiles in Fig. 7 show that within the dense slab ($-25 \le \tilde{x} \le 15$) the active and passive particles move together, $v_A(\tilde{x}) \approx v_P(\tilde{x}) \approx \langle V(t)\rangle/3$. Therefore, the MIPS kinetics in active–passive mixtures is neither a pure source/sink mechanism (in which the particles of the dense slab would remain at rest), nor a real drift of the particles at the full velocity $V(t)$, as if $\Delta_A = \Delta_P = 0$. Drift and source/sink act in parallel, self-maintained by the asymmetry of $\rho_\alpha(\tilde{x})$, which unbalance the local rectifications of the active forces at the front and back edges of the slab. With our $\rho(x,t) \approx \tilde{\rho}(x - \langle V\rangle t)$ hypothesis, if

$v_A(\tilde{x}) = v_P(\tilde{x})$ at a point $\tilde{x}$, their value is

$$v_A(\tilde{x}) = v_P(\tilde{x}) = \left(1 - \frac{\rho_T}{\rho_A(\tilde{x}) + \rho_P(\tilde{x})}\right)\langle V\rangle. \qquad (15)$$

The observed common velocities at the inner part of the MIPS slab ($\tilde{x} \approx 0$), $v_A(0) \approx v_P(0) \approx 0.2 \approx (1 - 2/3)\langle V\rangle$, are in good agreement with the total density profile in Fig. 3, being $\rho_T/(\rho_A(0) + \rho_P(0)) \approx 0.8/1.2 = 2/3$.

We now demonstrate how the system may develop the asymmetric density profiles, to produce a global force F_{PA} and self-sustain the movement $\langle V\rangle \neq 0$. In the ABP model the local rectification of the active force[31] produces the force density $f^a(\tilde{x})$ with positive/negative peaks at the back/front edges, compressing (*i.e.* stabilizing) the dense slab. The null total integral of $f^a(\tilde{x})$ is forced, on average, by the symmetry of the density profile. However, there are fluctuations such that $f^a(\tilde{x})$ becomes stronger at one edge, in correspondence to a sharper rise in $\rho_A(\tilde{x})$. Such fluctuation pushes the dense band in one direction and the front edge would sweep particles from the low-density phase. In the pure $\eta_P = 0$ case, the addition of more particles at the advancing edge would make stronger the rectification of the active force, thus compensating for the initial asymmetry. The short persistence time $\tau_p \approx 1.8$ reflects that kind of structural fluctuations, also observed in our binary mixtures.

In a mixture, the sweeping effect at the advancing edge would be stronger for the (lower mobility) passive particles. That would decrease the local concentration of the (higher mobility) active particles and the (backwards) rectified active force at the advancing edge, enhancing the initial force/density unbalance. Thus, the global motion of the slab may increase, against the friction of the Brownian dynamics.

At a given passive particle concentration η_P, a fluctuation might appear in the system with a typical time $\tau_o(\eta_P)$: this fluctuation could be strong enough to drive the system into a steady-state motion, with asymmetric density profiles and (action/reaction) opposite global forces on the two species. Eventually, with a typical time $\tau_{SMP}(\eta_P) \gg \tau_p$, another large fluctuation could break the self-sustained unbalance, leading to the end of the SMP.

5 Size effect analysis

The above analysis underlines the crucial role of passive particles as a reactive bath in which the local rectification of the active forces may produce not only MIPS but also the self-sustained asymmetry and the steady motion of the dense band. Since the unbalanced rectification of $f_A(\tilde{x})$ at the edges of the slab has to produce the real motion of all particles within, the SMPs are strongly size-dependent.

Fig. 8 presents $X(t)$ values for several simulations characterised by $\eta_P = 0.4$ and $\rho_T = 0.8$, but different sizes: $L_x = 100\sigma$ and $L_y = 25\sigma$ (a, blue); $L_x = 400\sigma$ and $L_y = 50\sigma$ (b, purple); $L_x = 400\sigma$ and $L_y = 100\sigma$ (c, orange); and $L_x = 200\sigma$ and $L_y = 50\sigma$ (d, red), which corresponds to the size used in all previous figures.

The smallest system (in blue, panel (a)) has the box lengths (L_x,L_y) and also the slab thickness (L_s), reduced to half of their

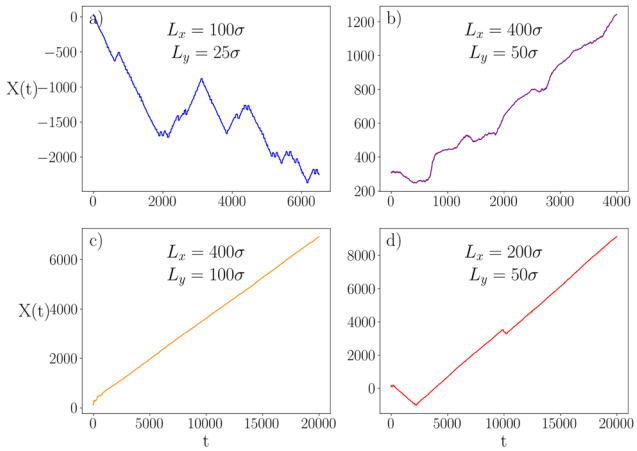

Fig. 8 Trajectories of MIPS bands ($X(t)$) with $\eta_P = 0.4$ for systems of different sizes at a fixed density $\rho = 0.8$ are shown. The trajectories correspond to the following system sizes: panel a, blue, $L_x = 100\sigma$ and $L_y = 25\sigma$ ($N_T = 2070$); panel b, purple, $L_x = 400\sigma$ and $L_y = 50\sigma$ ($N_T = 16\,110$); panel c, orange, $L_x = 400\sigma$ and $L_y = 100\sigma$ ($N_T = 32\,220$); and panel d, red, $L_x = 200\sigma$ and $L_y = 50\sigma$ ($N_T = 8055$), the same simulation as in panel (d) of Fig. 2.

values in the (original) system in panel (d). The $X(t)$ trajectory in the smallest system shows an SMP as clear as in the original (larger) system, but with a ($\pm$) velocity $V_{SMP} \approx 1.04$, *i.e.* much faster than the value $V_{SMP} \approx 0.57$ of the original system for the same η_P. That is expected since the total force unbalance has to scale as L_y, since it comes from the interfaces. In contrast, the friction of the Brownian bath has to scale as the total number of particles $N_T = 0.8L_xL_y$. Notice that, even taking into account that the results of the smallest system are reported over a longer trajectory than those of the larger one, its typical times seem to be shorter (since we observe several U-turns instead of the single U-turn observed in the large system). A quantitative estimate of the size dependence of τ_{SMP} and τ_o would require extremely large simulations, to get a good statistical sampling of these rare events. However, we might expect longer time scales in larger systems, since they need a larger fluctuation to create or destroy a SMP.

The other two panels in Fig. 8 show the results of simulations in systems larger than the original one (reported in panel d). In panels (b) and (c) L_x and the slab thickness L_s are twice as large as in (d). In panel (b) (purple line) we keep the original value of L_y, to get a more elongated aspect ratio for the MIPS band. We observe that after a long equilibration time the slab takes a positive velocity with $\langle V(t)\rangle \approx 0.3$, *i.e.* about half the value of the SMP in the original system (d): this is consistent with having similar interfacial forces ($\sim L_y$) against double friction effects ($\sim N_T \sim L_xL_y$). Thus, the increase of L_x and of the slab thickness L_s leads to $V(t)$ with much larger fluctuations around its mean (SMP) value, alternating fairly long periods characterised by a slab velocity clearly higher or lower than 0.3. Thus, the clean separation of the trajectories in the SMP, with $V(t) \approx \pm V_{SMP}$, divided by static periods with $\langle V(t)\rangle_t \approx 0$, breaks down. This could be caused by the fact that the longer L_x and L_s allow for enough free space for the appearance of frequent fluctuations that break the slab. Thus, our description in terms of the single variable $X(t)$ fails.

Panel (c) (orange line) corresponds to a system with the same L_x and slab thickness L_s as in panel (b), but L_y which is twice as large as in (d) (as a consequence, N_T is four times the original value). The trajectory $X(t)$ has (as in panel (b)) a long equilibration period followed by a steady forward motion of the dense slab, with a mean velocity $\langle V(t)\rangle \approx 0.34$ that is just slightly higher than in panel (c) (the system in panel (c) has twice as much interface than in panel (b), and twice as much N_T, *i.e.* friction from the bath). Even though the larger L_y size reduces the fluctuations of $V(t)$ around that mean value, we still cannot split the trajectory in panel (c) into SMP as cleanly as in the original system. Thus, we may interpret that the larger L_z = 100 makes it less likely than with L_y = 50 that a fluctuation splits the dense slab into two bands so that the description *via* the variable $X(t)$ (*i.e.* assuming a single dense band) is more accurate than in panel (b).

The size effects in $\langle V\rangle$ are directly transmitted to the mean particle velocities. Thus, compared to the values $\langle v_A\rangle = -0.03$ and $\langle v_P\rangle = 0.05$ achieved the original size (panel (d)), in the larger system (orange panel (c)) with ($\langle V\rangle = 0.34$), we obtain that the velocities of each species are $\langle v_A\rangle \approx -0.02$ and $\langle v_P\rangle \approx 0.03$. Very similar values are obtained when we duplicate L_x keeping the original value of L_y. Therefore, we conclude that the velocity of the slab is (roughly) inversely proportional to the x-length, such that $\langle V\rangle \propto \langle v_x\rangle \propto 1/L_x$ and $V_{SMP} \propto \langle v_x\rangle \propto 1/L_x$.

6 Analysis of U-turn events

The whole phenomenology described so far has to be interpreted as the appearance of mesoscopic structures, with large spatial and temporal scales that emerge by the presence of passive particles in ABP systems. In general, we may expect complex kinetic behaviours consisting of large and fast moving clusters colliding, merging and splitting. It is only through our choices for L_x and L_y, that we have been able to describe the phenomenology observed using the mesoscopic variable $X(t)$ and the time averages with $\tau_p \ll \Delta t < \tau_{SMP}(\eta_P)$.

The analysis of the events creating and destroying the SMP has to be restricted to shorter time averages and noisier density profiles. Fig. 9-panel (a) represents a zoom-in of the U-turn observed in Fig. 2-panel d at $t \approx 1500$ ($\eta_P = 0.4$) (see also Video in SM Vid_SP_U-turn_v2.mp4, ESI†).

The initial structure, with $V(t) = -V_{SMP}$, is characterised by the asymmetry reported in Fig. 3. Zooming in, panels (b)–(e) in Fig. 9 present the mean density profiles of active (continuum) and passive (dashed) particles along the U-turn: clearly, the density of the structure is highly disordered, as shown by the appearance of a region with relatively low density of active particles at the middle of the dense slab.

The (nominal) position of the slab $X(t)$, from eqn (4), reflects that a fluctuation period (nearly flat, in blue and in panel b) is followed by a much faster period (in red and in panel c). In fact, the trajectory $X(t)$ itself does not give a reliable representation of the actual kinetics. The Video in the ESI† shows that the dense slab is broken into two pieces (panel c) that move in opposite directions until, due to periodic boundaries, they collide again.

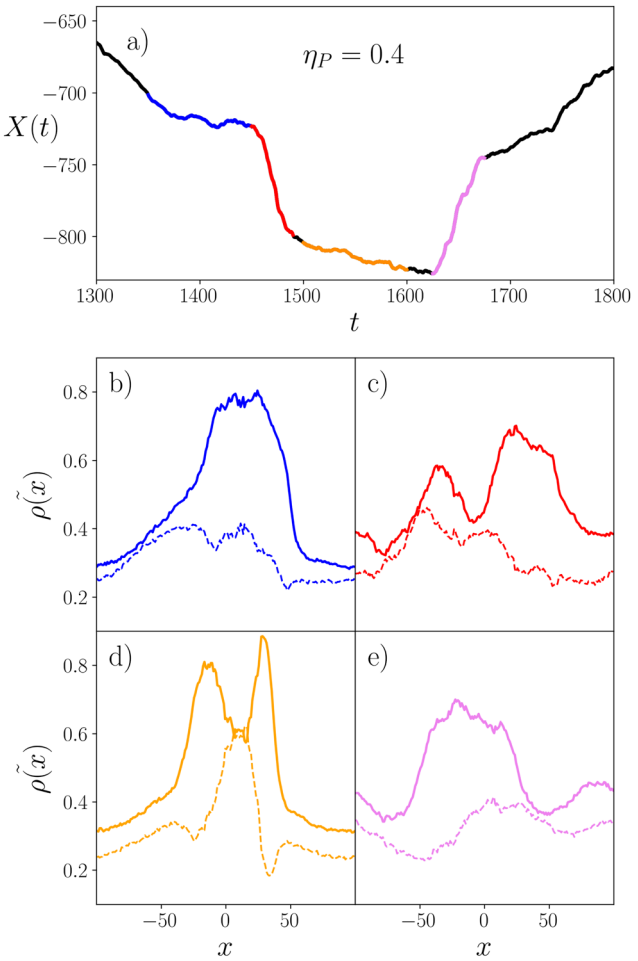

Fig. 9 (a) Zoom of the slab centre of the mass position ($X(t)$) of the η_P = 0.4 mixture in Fig. 2-panel (d), undergoing a U-turn. Panels (b)–(e) show the mean density profiles of the different intermediate states in panel a between the change of motion. Active particle density is represented with continuum lines and the passive one with dashed lines. The colour code in panels (b)–(e) refers to the colours along the line in panel (a).

Finally, the system reaches a nearly static structure over a period of $\Delta t \sim 1000$ (in orange and in panel d), in which the density profiles are (nearly) symmetric, with a very high density of passive particles at the centre. Reversing the sequence of events for $t < 1500$, $X(t)$ has a sudden acceleration (in purple and in panel e) in which the left-right symmetry is broken, to reach a SMP with $V(t) = V_{SMP}$.

Thus, the large fluctuations that create and destroy the SMP in our simulations overcome our effort, in eqn (4)–(6), to describe the MIPS structure as a single cluster at the position $X(t)$.

7 Discussion and conclusions

In a pure system of active Brownian particles, the motion of particles (induced by the thermal agitation, the active and the

interaction forces) is damped by the inert bath, that acts independently on each particle. The addition of repulsive passive particles to ABP systems provides a reactive bath for the active ones. The clustering of active particles in MIPS induces inhomogeneous distributions of the passive particles that would be reflected in the motion of the active ones. Fluctuations that break the $(\pm x)$ symmetry may create total (opposite) forces that particles of each species induce on those of the other species. Their opposite fluxes on the MIPS less-dense phase may lead to a self-sustained motion of the dense band, by a combination of sink-source effects at the edges and a global shift of the (much rigid) inner dense slab.

To characterize and quantify all these effects, we have used simulations of a mixture of active/passive Brownian particles in a simple geometry: dense bands that cover the full period L_y, along the (shorter) Y axis, and move along the (longer) X axis, so that we may define a variable $X(t)$ to localize the position of the dense slab and $V(t)$ for its velocity. In terms of these mesoscopic variables, we observe the emergence of characteristic time scales, much larger than the autocorrelation time τ_p for $V(t)$ in pure ABP systems. Steady moving structures (either with positive or negative mean velocity, $X(t) - X(t_o) \approx \pm V_{SMP}(\eta_P)(t - t_o)$) appear with a typical time $\tau_o(\eta_P)$ and persist for a typical time $\tau_{SMP}(\eta_P)$ that may be very long. In our simulations we get fairly accurate estimations for $V_{SMP}(\eta_P)$ in mixtures with different compositions $0.2 \leq \eta_P \leq 0.4$, and for different sizes of the simulation box.

The self-assembly and motion of the MIPS clusters is a mesoscopic phenomenon, depending on the size and geometry of the dense cluster and on the distance between its two edges through the less dense phase (across the periodic boundary conditions). The U-turn events observed in our simulations, when the motion of the dense slab is reversed, correspond to fluctuations that break the slab into two pieces. If the slab is too elongated (large aspect ratio L_s/L_y) these events may become frequent, with small pieces of slab breaking out of the main cluster, at one or the other edge, with the result of a worse defined velocity $\pm V_{SMP}$. On the other hand, larger values of L_y give longer persistence times τ_{SMP}, for the steady motion of the slab.

We compute statistical averages over (long) time intervals in which $X(t)$ keeps the same linear trend (either with $V(t) \approx \pm V_{SMP}(\eta_P)$), in terms of particle positions relative to the slab's mesoscopic position $X(t)$. This allows us to obtain density, force and velocity profiles characterizing the kinetics and dynamics of the moving structures. All these variables contribute to the generic terms of the Smoluchoski equation for Brownian particles. The generic mechanism to achieve steady motion is that active particles push (and are pushed by) passive particles, producing stationary density and velocity profiles, in terms of the variable $\tilde{x} = x - X(t)$, reflecting (and producing) a global inter-species force $F_{AP} = -F_{PA} \neq 0$, either positive or negative.

Thus, the spontaneous breakage of the (spatial x and temporal t) symmetry cannot appear in a pure ($\eta_P = 0$) ABP system. Thus, we might consider the passive particle concentration η_P as the parameter to turn on the most primitive features of hydrodynamics, when collective motions of swimmers are made possible by their global push on a reactive medium. Our detailed statistical analysis for the different kinetic regimes (steady moving structures and the rare events that produce their U-turns) allowed us to interpret their dynamics within the framework of the Smoluchowski equation for interacting Brownian particles, thus providing a clearer physical perspective on MIPS.

The dynamics of the MIPS in active–passive mixtures under different conditions is likely to be much complex, with entangled effects of the different kinetic regimes we have identified and analysed. Nevertheless, we hope that our analysis underlines the essential role of passive particles, allowing for the time-space symmetry breaking, over time scales much larger than the typical fluctuations in ABP, and based on a self-sustained combination of a collective drift of particles in a cluster with local source/sink effects at the edges, leading to the structures' kinetics apparently faster than the actual particles' mean motion. As far as we are aware, so far experimental realizations of MIPS have dealt with confined systems. However, in order to observe the experimental equivalent of a travelling band, one might need to be able to implement a cylindrical geometry in an experimental setup.

Data availability

The data that support the findings of this study will be available upon request from Chantal Valeriani, on behalf of all authors.

Conflicts of interest

There are no conflicts to declare.

Acknowledgements

We acknowledge the support from the Spanish Secretariat for Research, Development and Innovation (grants no. PID2020-117080RB-C52, PID2022-139776NB-C66, IHRC22/00002 and PID2022-140407NB-C21) and the Maria de Maeztu Programme for Units of Excellence in R&D (CEX2023-001316-M).

Notes and references

1 M. E. Cates and J. Tailleur, *Europhys. Lett.*, 2013, **101**, 20010.
2 A. Martin-Gomez, D. Levis, A. Diaz-Guilera and I. Pagonabarraga, *Soft Matter*, 2018, **14**, 2610.
3 P. Digregorio, D. Levis, A. Suma, L. F. Cugliandolo, G. Gonnella and I. Pagonabarraga, *Phys. Rev. Lett.*, 2018, **121**, 098003.
4 C. B. Caporusso, P. Digregorio, D. Levis, L. F. Cugliandolo and G. Gonnella, *Phys. Rev. Lett.*, 2020, **125**, 178004.
5 J. Stenhammar, D. Marenduzzo, R. Allen and M. Cates, *Soft Matter*, 2014, **10**, 1489.
6 J. J. Bialke, J. T. Siebert, H. Lowen and T. Speck, *Phys. Rev. Lett.*, 2015, **115**, 098301.

7 A. K. Omar, Z.-G. Wang and J. F. Brady, *Phys. Rev. E*, 2020, **101**, 012604.
8 C. Bechinger, R. D. Leonardo, H. Lowen, C. Reichhardt, G. Volpe and G. Volpe, *Rev. Mod. Phys.*, 2016, **88**, 045006.
9 G. S. Redner, M. F. Hagan and A. Baskaran, *Phys. Rev. Lett.*, 2013, **110**, 055701.
10 M. E. Cates and J. Tailleur, *Annu. Rev. Condens. Matter Phys.*, 2015, **6**, 219–244.
11 A. Wysocki, R. G. Winkler and G. Gompper, *Europhys. Lett.*, 2014, **105**, 48004.
12 J. Martin-Roca, R. Martinez, L. Alexander, A. Diez, D. Aarts, F. Alarcon, J. Ramírez and C. Valeriani, *J. Chem. Phys.*, 2021, **154**, 164901.
13 M. James, E. Clément, J. Robert and B. Maria, *Proc. R. Soc. A*, 2023, **479**, 20230524.
14 X. q Shi, G. Fausti, H. Chate, C. Nardini and A. Solon, *Phys. Rev. Lett.*, 2019, **125**, 168001.
15 D. Levis, J. Codina and I. Pagonabarraga, *Soft Matter*, 2017, **13**, 8113.
16 L. Caprini, E. Hernandez-Garcia, C. Lopez and U. M. B. Marconi, *Sci. Rep.*, 2019, **9**, 16687.
17 A. P. Solon, J. Stenhammar, M. E. Cates, Y. Kafri and J. Tailleur, *New J. Phys.*, 2018, **20**, 075001.
18 A. Wysocki, R. G. Winkler and G. Gompper, *New J. Phys.*, 2016, **18**, 123030.
19 E. Tjhung, C. Nardini and M. E. Cates, *Phys. Rev. X*, 2018, **8**, 031080.
20 S. Hermann, D. de las Heras and M. Schmidt, *Mol. Phys.*, 2021, **119**, e1902585.
21 G. Gonnella, D. Marenduzzo, A. Suma and A. Tiribocchi, *C. R. Phys.*, 2015, **16**, 316.
22 I. Buttinoni, J. Bialke, F. Kummel, H. Lowen, C. Bechinger and T. Speck, *Phys. Rev. Lett.*, 2013, **110**, 238301.
23 S. Thutupalli, R. Seemann and S. Herminghaus, *New J. Phys.*, 2011, **13**, 073021.
24 D. D. Nishiguchi and M. Sano, *Phys. Rev. E: Stat., Nonlinear, Soft Matter Phys.*, 2015, **92**, 052309.
25 G. Briand and O. Dauchot, *Phys. Rev. Lett.*, 2016, **117**, 098004.
26 J. Bialké, J. T. Siebert, H. Löwen and T. Speck, *Phys. Rev. Lett.*, 2015, **115**, 098301.
27 A. Patch, D. M. Sussman, D. Yllanes and M. C. Marchetti, *Soft Matter*, 2018, **14**, 7435–7445.
28 N. Lauersdorf, T. Kolb, M. Moradi, E. Nazockdast and D. Klotsa, *Soft Matter*, 2021, **17**, 6337–6351.
29 S. Hermann, D. de las Heras and M. Schmidt, *Phys. Rev. Lett.*, 2019, **123**, 268002.
30 E. Chacon and P. Tarazona, *J. Phys.: Condens. Matter*, 2005, **17**, S3493.
31 E. Chacon, F. Alarcon, J. Ramírez, P. Tarazona and C. Valeriani, *Soft Matter*, 2022, **18**, 2646.
32 R. Matas-Navarro, R. Golestanian, T. B. Liverpool and S. M. Fielding, *Phys. Rev. E*, 2014, **90**, 032304.
33 M. Theers, E. Westphal, K. Qi, R. G. Winkler and G. Gompper, *Soft Matter*, 2018, **14**, 8590–8603.
34 H. Zhao, A. Košmrlj and S. S. Datta, *Phys. Rev. Lett.*, 2023, **131**, 118301.
35 H. Lowen, *J. Chem. Phys.*, 2020, **152**, 040901.
36 J. Su, H. Jiang and Z. Hou, *New J. Phys.*, 2021, **23** 013005.
37 C. M. Barriuso, C. Vanille, F. Alarcon, I. Pagonabarraga, R. Brito and C. Valeriani, *Soft Matter*, 2021, **17**, 10479.
38 F. Dittrich, T. Speck and P. Virnau, *Eur. Phys. J. E*, 2021, **44**, 53.
39 S. Dikshit and S. Mishra, *Eur. Phys. J. E: Soft Matter Biol. Phys.*, 2022, **45**, 21.
40 B.-Q. Ai, B.-Y. Zhou and X.-M. Zhang, *Soft Matter*, 2020, **16**, 4710–4717.
41 Y. Wang, Z. Shen, Y. Xia, G. Feng and W. Tian, *Chin. Phys. B*, 2020, **29**, 053103.
42 F. Hauke, H. Löwen and B. Liebchen, *J. Chem. Phys.*, 2020, **152**, 014903.
43 C. Valeriani, M. Li, J. Novosel, J. Arlt and D. Marenduzzo, *Soft Matter*, 2011, **7**, 5228–5238.
44 X.-L. Wu and A. Libchaber, *Phys. Rev. Lett.*, 2000, **84**, 3017–3020.
45 G. Grégoire, H. Chaté and Y. Tu, *Phys. Rev. Lett.*, 2001, **86**, 556.
46 A. E. Patteson, A. Gopinath and P. E. Arratia, *Nat. Commun.*, 2018, **9**, 5373.
47 D. R. Rodriguez, F. Alarcon, R. Martinez, J. Ramrez and C. Valeriani, *Soft Matter*, 2020, **16**, 1162.
48 J. Stenhammar, R. Wittkowski, D. Marenduzzo and M. E. Cates, *Phys. Rev. Lett.*, 2015, **114**, 018301.
49 A. P. Thompson, H. M. Aktulga, R. Berger, D. S. Bolintineanu, W. M. Brown, P. S. Crozier, P. J. in't Veld, A. Kohlmeyer, S. G. Moore, T. D. Nguyen, R. Shan, M. J. Stevens, J. Tranchida, C. Trott and S. J. Plimpton, *Comput. Phys. Commun.*, 2022, **271**, 108171.
50 J. D. Weeks, D. Chandler and H. C. Andersen, *J. Chem. Phys.*, 1971, **54**, 5237–5247.
51 F. Penna and P. Tarazona, *J. Chem. Phys.*, 2003, **119**, 1766–1776.

